Coordination Chemistry Reviews 253 (2009) 2363–2375

Contents lists available at ScienceDirect

Coordination Chemistry Reviews

journal homepage: www.elsevier.com/locate/ccr

Review

High-spin Co(II) in monomeric and exchange coupled oligomeric structures: Magnetic and magnetic circular dichroism investigations

S. Ostrovsky[a,b], Z. Tomkowicz[a,c], W. Haase[a,*]

[a] Eduard-Zintl-Institute of Inorganic and Physical Chemistry, Darmstadt University of Technology, Petersenstrasse 20, 64287 Darmstadt, Germany
[b] Institute of Applied Physics, Academy of Sciences of Moldova, Academy Str. 5, 2028 Chisinau, Moldova
[c] Institute of Physics, Jagiellonian University, Reymonta 4, 30-059 Krakow, Poland

Contents

ARTICLE INFO

Article history:
Received 14 August 2008
Accepted 18 October 2008
Available online 30 October 2008

Keywords:
Co(II) complexes
Zero field splitting
Spin–orbit coupling

ABSTRACT

The Co(II) ion is a good spectroscopic probe to study the electronic structure of the active centers of metalloenzymes. Especially interesting are magnetic properties of the high-spin Co(II) ion because of the complexity resulting from an unquenched orbital angular momentum. The objectives of this contribution are high-spin Co(II) monomers, dimers and linear trimers in various coordination. Magnetic data, reported in literature, for the high-spin Co(II) complexes are reviewed. The investigation of some selected high-spin Co(II) monomers, both in distorted tetrahedral and octahedral coordination, and several distorted octahedral coordinated dimers and linear trimers is presented. Special attention is paid to the internally exchange coupled Co(II) dimers and linear trimers. The complete experimental data set, consisting of the temperature dependent magnetic susceptibility, the magnetic field dependent magnetization and the variable

Abbreviations: ZFS, zero field splitting; MCD, magnetic circular dichroism; TIP, temperature independent paramagnetism; μ-AA, bridging acetohydroxamate anion; μ-BA, bridging benzohydroxamate anion; tmen, *N,N,N′,N′*-tetramethylethylenediamine; μ-OAc, bridging acetate group; OAc, single bonded acetate group; $\mu\text{-}OAc_F$, bridging trifluoroacetate group; OAc_F, single bonded trifluoroacetate group; $\mu\text{-}OAc_{Cl}$, bridging trichloroacetate group; OAc_{Cl}, single bonded trichloroacetate group; OTf, triflate.

* Corresponding author. Tel.: +49 6151 16 3398; fax: +49 6151 16 4924.
E-mail address: haase@chemie.tu-darmstadt.de (W. Haase).

0010-8545/$ – see front matter
doi:10.1016/j.ccr.2008.10.015

Magnetic circular dichroism (MCD)
Magnetic measurements
Magnetization

temperature – variable field – magnetic circular dichroism (VTVH-MCD) is the powerful basis for extracting important electronic parameters such as zero field splitting (ZFS) and exchange coupling constant values. The data obtained for the exchange constant and the ZFS parameters are correlated to the environment of the Co(II) ion and the bridging fragments. Theoretical analysis is performed on the base of different models and under which conditions the simple spin-only Hamiltonian can be applied or when the orbital angular momentum must be included into consideration. The applicability of ZFS parameter as an indicator for the kind of coordination is discussed. The magnetic, magnetization and MCD investigations accompanied by theoretical calculations complement each other. Using the three independent experimental techniques, the parameters extracted for each individual method can be crosschecked.

1. Introduction

Among 3d transition metal elements, difficulties are encounted analyzing the magnetic data of the high-spin ($S = 3/2$) $3d^7$ Co(II) ion. In octahedral coordination some challenges exist due to the presence of unquenched orbital angular momentum [1–3]. For tetrahedral coordination the situation is much easier since the ground state is orbitally non-degenerate and the analysis is based on the spin-only Hamiltonian. The contributions from the orbital angular momentum are fully included into consideration in terms of zero field splitting (ZFS) tensor and anisotropic *g*-factor. In many cases this spin-only Hamiltonian is also used for octahedrally coordinated Co(II), assuming that the distortion from the octahedral environment is strong enough to remove the orbital degeneracy. In other words, the spin-only Hamiltonian can be used only when a strong distortion splits the orbital triplet leading to stabilization of the orbital singlet. If the distortion is not strong enough or the orbital doublet is lowest in energy, the ZFS approach cannot be used and the orbital angular momentum must be included into consideration.

The value of the ZFS parameter *D* has been considered as an important indicator for the kind of coordination [4]. Whereas for octahedral coordination, *D* could be up to 100 cm^{-1} (or even more), for tetrahedral coordination *D* values are moderate, up to around 10 cm^{-1} [5]. Surprisingly, *D* values of 100 cm^{-1} were reported even for a high-spin tetrahedral Co(II)–thiolate complex [5]. Fivefold coordinated Co(II) complexes have *D* values about 70 cm^{-1} [6]. Unfortunately, in reality the *D* parameter is not an ideal coordination number indicator because of significant overlapping of particular *D* intervals.

When exchange coupled dimers or oligomers are considered, the situation is even more complicated since, in general, the exchange interaction between high-spin Co(II) ions could be anisotropic. In addition, since in many cases the ZFS is bigger than the exchange interaction, it is not easy to separate the contributions of different interactions. It is evident a broad variety of independent experimental results is a powerful basis for extracting the needed parameters.

One easy distinction between octahedral and tetrahedral coordination is the spectroscopic behavior, the frequency, the absorption intensity and as a result, the color [7]. For octahedral environment the color is pink with absorption maximum near 530 nm but, for tetrahedral coordination the color is blue with absorption maximum near 650 nm. On the other hand, the distinction between four- and five-coordinate systems is sometime not easy [8]. Even the distinction between five- and six-coordinate systems can create some problems.

In some complexes the Co(II) ion can appear simultaneously in two coordination sites, as shown for *Escherichia coli* methionyl aminopeptidase [9] using magnetic circular dichroism (MCD). Researchers were able to differentiate between six- and fivefold coordinated Co-ions by analyzing the temperature and field dependent behavior of two major peaks (at 495 and 567 nm) and supporting assignment with the help of the angular overlap method (AOM). Interestingly, the MCD spectrum of Co(II) in *E. coli* alkaline phosphatase [10] is dominated by an absorption maximum at 540 nm, interpreted as due to distorted tetrahedral coordination, while a wing at about 500 nm is attributed to additional Co(II) ions in octahedral symmetry.

MCD spectroscopy [11] is a very powerful method to characterize high-spin Co(II) monomers as well as oligomers. This technique is popular in biochemistry due to the possibility of determination of the intrinsic geometry and the electronic structure of the active centers in metalloenzymes. Cobalt ion being in the active center is the valuable probe to study enzymatic activity. Selected MCD spectra for Co monomers in typical tetrahedral coordination for Co(II) metalloenzyms were presented in Ref. [12] and for low molar mass Co(II) compounds in Ref. [13]. Typical spectra for the octahedral coordination can be found in Ref. [12b].

The metalloenzymes most studied are those which possess iron in their active center. Naturally occurring cobalt metalloenzymes are not so common as iron metalloenzymes, but cobalt can replace other metal ions in some native metalloenzymes with partial or full retention of their activity, as, e.g., Zn(II) in carbonic anhydrase [14], in horse liver alcohol dehydrogenase [15] or in insulin hexamer [16]. By substituting Cu, binuclear Co centers can be formed as in the case of cobalt hemocyanin [17,18] and can be investigated by MCD spectroscopy [18]. For such binuclear complexes, magnetic interactions are possible. These interactions are very sensitive to the kind of bridge, which can be influenced during the catalysis reaction with substrates or during reaction with inhibitors. This can create new possibilities to study enzymatic activity.

Very recently Johansson et al. [19] synthesized some dicobalt II–II, II–III and III–III complexes with the aim to study their spectroscopic and magnetic properties as models for dicobalt enzyme active sites. Particular attention was devoted to the complex containing two Co(II) ions, both with distorted octahedral coordination. The peaks observed in the MCD spectra in the low wavelength region (300 nm) were assigned to ligand to metal charge transfer transitions. The temperature dependent broad maximum near 500 nm was interpreted as due to transitions from the ground $^4A_2$ state to the excited $^4T_1$ (P) state, split by distortion and spin–orbit coupling. All peaks in the spectra were temperature dependent and assigned to C terms with some admixture of B terms. Temperature and magnetic field dependence of MCD peaks and magnetic data were interpreted, assuming full freezing of orbital moment and resulting in a weak antiferromagnetic coupling $J_{ex} = -1.6$ cm^{-1} [1] between the Co(II) centers with $D = 44$ cm^{-1} and isotropic Landé-factor $g = 2.4$.

Another powerful method to determine ZFS has recently been developed. This is high frequency, high field EPR (HFEPR), which is a direct method to obtain ZFS by measuring an inter-Kramers transition [4a,20]. The values of *D* parameter up to 30 cm^{-1} can be

[1] We use the following convention with a factor 2: $H = -2J_{ex}S_iS_j$.

measured with this technique. This is, however, much less than that measured with the MCD method (up to about 100 cm^{-1}). There are examples of using both HFEPR and VTVH-MCD [15,20a]. Whereas in Ref. [15] VTVH-MCD was used as completion of the conventional EPR study, in Ref. [20a] HFEPR was compared with MCD and the results obtained from both methods were in a good agreement. While HFEPR is more accurate, MCD is more sensitive for extracting the ZFS parameters.

Conventional X-band EPR is also in use. However, the evaluation of ZFS from these EPR measurements is not easy. Three resolved signals on the spectrum are needed, corresponding to effective g-factors: g'_x, g'_y, g'_z, from which one can calculate E/D value (see one example [15]) and use some formula to extract E and D; here E is the rhombic zero field splitting and D the axial one. One other limitation is due to the fact that the splitting energy is sometimes greater than the microwave energy, in particular by using X-band spectrometer.

The most commonly used method to obtain ZFS and to characterize the magnetic properties is measuring the magnetic susceptibility vs. temperature and magnetization vs. field. Some selected papers are quoted below where, for high-spin Co(II) uncoupled (monomers) and exchange coupled complexes (dimers and linear trimers), the analysis of the magnetic data was performed mostly by taking the orbital moment into account. The contributions of our group in that field will be referred to in the following sections.

Let us begin with $Co[HO_2C(CH_2)_3NH(CH_2PO_3H)_2]_2$. This carboxylate-phosphonate has been synthesized and characterized by Yang et al. [21]. Neighboring CoO_6 octahedra are interconnected into a 2D layer and the compound shows a phase transition at T_c = 8.75 K. Nevertheless, using data above T_c it was possible to extract parameters of individual Co(II) ions. The interaction between Co-ions was taken into account in the molecular field approximation. The χT value at 300 K was 3.36 emu K/mol, much higher than the pure spin-only value (equal to 1.87 emu K/mol with g = 2). The susceptibility was analyzed by the spin–orbit model assuming pure octahedral symmetry of the crystal field.

Duggan and Hendrickson [22] analyzed the magnetic data of some five-coordinate Co monomers taking the spin–orbit interaction into account. Magnetic data for two five- and one six-coordinate exchange interacting dimers were also analyzed, but, the spin-only approach was used. Quite small negative values of exchange constants were obtained.

Herrera et al. [23] described a compound composed of magnetically isolated Co(II) ions in the distorted octahedral diamagnetic N_4O_2 environment $[W^{IV}\{(\mu\text{-}CN)_4Co^{II}(H_2O)_2\}\cdot 4H_2O]_n$. This compound was analyzed using a Hamiltonian with spin–orbit coupling and axial distortion. The obtained axial crystal field splitting parameter Δ was 100 cm^{-1} and the $\chi T/2$ value at 300 K was 2.72 emu K/mol.

Co(II) dimers surrounded by different macrocycles were reported in Ref. [24] using the isotropic HDvV model. A different macrocycle was used by Caneschi et al. [25] considering a modified Hamilton operator in order to describe the spin–orbit contribution.

De Munno et al. [26] studied three bipyrimidine-bridged homodinuclear complexes. In two of these complexes Co-ions have slightly distorted octahedral coordination with terminal aqua and two N ligands. In the third complex the coordination is also octahedral with all N ligand atoms belonging to two thiocyanate and two bipyrimidine groups. For all these complexes, the value of J_{ex} obtained was about −2.5 cm^{-1}. Other pyrimidine-containing cobalt(II) coordination polymers were presented by Fabelo et al. in a very recent contribution [27].

Aromi et al. studied [28] two di- and one trinuclear complexes of hexacoordinate Co(II) of a bis-β-diketone ligand with three different conformations. The magnetic data were treated using models that include spin–orbit coupling effects. The values of J_{ex} obtained were 0 cm^{-1}, +0.11 cm^{-1} for dimers and J_{ex} = −1.2 cm^{-1} for trimer.

In Ref. [29] the magnetic properties of a linear tetrahedral Co trimer $Co_3[NH_2(CH_2PO_3)_2]_2$ were analyzed. The $\chi T/3$ value obtained at 300 K was 2.57 emu K/mol, higher than expected for the spin-only value. This is an indication of an admixture of excited states to the ground one by the spin–orbit coupling. A linear trinuclear Co(II) complex $Co_3(NCS)_6(admtrz)_6\cdot CH_3OH\cdot H_2O$ with triazolate bridges was presented in Ref. [30a] using the simplified HDvV model. Several other linear Co(II) trimers were described in Refs. [30b,c,d]. High-spin Co(II) in layered structures was presented in [31], where ZFS data were extracted from magnetic and EPR measurements.

Cobalt complexes are interesting not only from the biochemical point of view. Cobalt can show very high anisotropy because of a not completely frozen orbital moment. This is important for the design of new devices for use in information storage. Due to their high anisotropy, polynuclear Co complexes are good candidates for single molecule magnets, e.g. the hexanuclear Co(II) complex $[Co_6(OH)_2(L)_{10}]$ (L = phenylcinnamate) synthesized by Kumagai et al. [32]. This complex containing two octahedral and four tetrahedral Co(II) ions was studied by magnetic and MCD measurements. The MCD spectrum is dominated by tetrahedral ions. The total spin value of the ground state was determined to be S = 3. Information about anisotropy was not given. Two Co-complexes which behave as SMM [33] are a citrate cubane [33a] and a hexanuclear citrate [33b] containing the cubane core, both of which show an energy barrier for reorientation of magnetization of about ∼20 cm^{-1}. The presence of AFM interactions and ZFS was qualitatively stated but no quantitative analysis of the susceptibility data was given.

Semi quantitative theoretical models will be referred in the following section. On this stage, we quote only the early work [34], were the principal magnetic susceptibilities of exchange coupled binuclear Co(II) species were treated. After a short section presenting the theoretical foundation, we will present our own results obtained by magnetic measurements usually combined with magnetization measurements, VTVH-MCD magnetization measurements and theoretical analysis. The parameters of the adequate Hamiltonian not containing or containing spin–orbit interaction are compared for different Co-complexes. As one of the main goals, VTVH-MCD experiments were tested in order to independently extract the magnetic parameters out of this method, especially the exchange coupling.

2. Theoretical background

2.1. Magnetic interactions

The Hamiltonian for the mononuclear high-spin Co(II) complex in an octahedral environment can be written as a sum of three parts: the spin–orbit interaction, the low symmetry crystal field operator and the Zeeman perturbation. We regard each part separately. The ground state of high-spin Co(II) ion in an octahedral environment is orbitally degenerate ($^4T_{1g}$ triplet in a cubic crystal field). Focusing on the $^4T_{1g}$ ground state only (corresponding with the assumption that the ligand field is strong enough), we can describe Co(II) as an ion with the spin value S = 3/2 and the fictitious angular momentum L = 1. The spin–orbit interaction within the $^4T_{1g}$ triplet can be written as follows:

$$\boldsymbol{H}_{SO} = -\frac{3}{2}\kappa\lambda\boldsymbol{SL}, \quad (1)$$

where κ is the orbital reduction factor and λ is the spin–orbit coupling parameter for a free Co(II) ion. The factor −3/2 appears

because the matrix elements of **L** within the $^4T_{1g}$ states are exactly the same as the matrix elements of $-3\mathbf{L}/2$ within the p basis. According to [1] $\lambda = -170\,cm^{-1}$. The orbital reduction factor κ takes into account not only the covalency of the cobalt–ligand bonds but also the mixture of both $^4T_{1g}$ states (originating from ^4F and ^4P). Neglecting covalency, we find that κ varies between 1 (weak-field limit) and 2/3 (strong-field limit).

For real compounds the symmetry is at best axial. The low symmetry field, that takes into account the distortion of the local environment, is significant for the explanation of the behavior of cobalt complexes. Combined with the spin–orbit interaction this low symmetry field gives rise to a strong magnetic anisotropy of the Co(II) ion. In general, the crystal field operator can be written in the following form:

$$\boldsymbol{H}_{Cr} = \boldsymbol{L}\boldsymbol{\Delta}\boldsymbol{L}. \tag{2}$$

The $\boldsymbol{\Delta}$ tensor describes the splitting of the $^4T_{1g}$ term in the local crystal field. In the coordinate system that coincides with the main axes of the $\boldsymbol{\Delta}$ tensor, the last one can be written as

$$\boldsymbol{\Delta}^{loc} = \begin{pmatrix} -\Delta/3 + E & 0 & 0 \\ 0 & -\Delta/3 - E & 0 \\ 0 & 0 & 2\Delta/3 \end{pmatrix} \tag{3}$$

Δ and E are the axial and rhombic parameters of the $\boldsymbol{\Delta}$ tensor. To obtain the $\boldsymbol{\Delta}$ tensor in arbitrary coordinate system, the unitary transformation must be performed:

$$\boldsymbol{\Delta} = \boldsymbol{\nu}^{-1}\boldsymbol{\Delta}^{loc}\boldsymbol{\nu}, \tag{4}$$

where $\boldsymbol{\nu}$ is the orthogonal transformation matrix.

There is a correspondence between the sign of Δ and the type of distortion. The ground state of the Co(II) ion in the octahedral environment represents a superposition of two $^4T_{1g}$ states, namely $|t_{2g}^5(^2T_{2g})e_g^2(^3A_2), ^4T_{1g}\rangle$ and $|t_{2g}^4(^3T_{1g})e_g^3(^2E_2), ^4T_{1g}\rangle$. The coefficients in this superposition depend on the strength of the crystal field; however, in any case the contribution of $t_{2g}^5e_g^2$ configuration is greater. So, it can be assumed that the behavior of the high-spin Co(II) ion with symmetry lowering is determined by the behavior of this electronic configuration. The axial distortion along local z-axis leads to the splitting of e_g and t_{2g} states. The compression leads to the stabilization of d_{xy} orbital, whereas for elongation d_{xz} and d_{yz} are the lowest in energy. The states obtained can be filled in with 7 d-electrons, and for the $t_{2g}^5e_g^2$ configuration the compression results in the doubly degenerate ground-state, whereas for the elongation there is no orbital degeneracy. Thus, in terms of Eqs. (2) and (3) the compression and the elongation of the local environment can be described with the negative and positive values of Δ parameter, respectively.

The Zeeman interaction for the high-spin Co(II) ion consists of both spin and orbital contribution and is

$$\boldsymbol{H}_{Ze} = \mu_B\left(g_0\boldsymbol{S} - \frac{3}{2}\kappa\boldsymbol{L}\right)\mathbf{H}. \tag{5}$$

μ_B and $g_0 = 2.0023$ are the Bohr magneton and the Landé factor for free electron, respectively. In Eq. (5), the spin–orbit interaction between the $^4T_{1g}$ ground state and any excited state is neglected. After accounting for this interaction [35] the g_0 value in Eq. (5) must be replaced by $g_0 + \Delta g$, where Δg depends on the Racah and cubic crystal field parameters as well as on the one-electron spin–orbit coupling constant. For the averaged values of these parameters for the high-spin Co(II) ion, Δg is about 0.12. As one can see, this value is small but not negligible. Accounting for the low-symmetry crystal field results in the anisotropy of the Δg value. However, for interpretation of magnetic properties this anisotropy can be neglected.

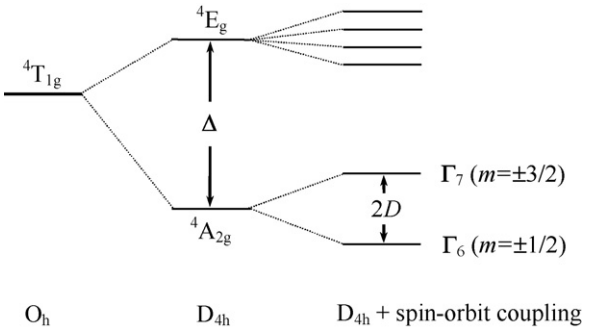

Fig. 1. Energy spectrum of Co(II) ion in the case of elongation along the tetragonal axis.

If the low symmetry crystal field is strong enough and Δ-parameter is positive, the orbital angular momentum disappears. The mononuclear octahedrally coordinated Co(II) complex can be regarded as a spin-only system with $S = 3/2$. The influence of orbital momentum is incorporated into the principal values of local zero-field splitting tensors on the one hand and local **g**-tensors on the other hand. The energy levels of mononuclear Co(II) complex in the case of positive Δ are schematically shown in Fig. 1. Labels correspond to the case of tetragonal distortion. Strong positive Δ leads to stabilization of 2 Kramers doublets with $m = \pm 1/2$ and $\pm 3/2$. Denoting the energy gap between these doublets by $2D$, one can describe the behavior of strongly distorted mononuclear octahedrally coordinated Co(II) complex with the following Hamiltonian:

$$\boldsymbol{H} = \boldsymbol{S}\boldsymbol{D}\boldsymbol{S} + \mu_B\boldsymbol{S}\mathbf{g}\mathbf{H}, \tag{6}$$

where ZFS $\boldsymbol{D}$-tensor in the main axes coordinate system can be written as Eq. (3) with D axial parameter, **g** is the Zeeman tensor. Typical values of D-parameter for octahedrally coordinated cobalt can be up to $100\,cm^{-1}$. Since in all ranges of the Δ-parameter the states with $m = \pm 1/2$ are lower in energy than the states with $m = \pm 3/2$, the axial D-parameter for Co(II) in octahedral environment is positive.

In the tetrahedral environment, the high-spin Co(II) ion possesses an orbitally non-degenerate ground state ($^4A_{2g}$ orbital singlet). The complex is described with the use of Hamiltonian Eq. (6), the D-parameter may be both positive and negative with an absolute value in general (see Introduction) smaller than $10\,cm^{-1}$.

Let us turn now to the complexes containing more than one magnetic center. For this type of compounds the exchange interaction between different centers is of great importance and must be included in the corresponding Hamiltonian along with the single ion interactions regarded above for the mononuclear high-spin cobalt complex. As long as the ground-state of Co(II) is orbitally degenerate, the exchange interaction between cobalt ions should contain, in general, both orbital and spin contributions. Some *ab initio* calculations performed for the binuclear chlorine bridged Co(II) complexes demonstrated that the energy pattern due to the exchange interaction cannot be described by the simple Heisenberg scheme [36]. The exchange Hamiltonian deduced on the base of microscopic approach for the corner shared bioctahedral Co(II) of D_{4h} symmetry [37] demonstrates that the exchange interaction in this complex is essentially anisotropic. However in many cases the approach of Lines [38] that exchange between cobalt centers contains only an isotropic part operating with the real spins leads to reasonable explanation of the properties of the corresponding complexes and the exchange part of the Hamiltonian can be written as

$$\boldsymbol{H}_{ex} = -2J_{ex}\boldsymbol{S}_i\boldsymbol{S}_j. \tag{7}$$

J_{ex} is the exchange coupling parameter and subscripts i and j refer to the interacting ions.

The magnetic properties of interacting Co(II) ions (especially at low temperatures) strongly depend on the relative orientation of the principal axes of the local $\mathbf{\Delta}$ tensors. Sometimes the directions of these axes can be predicted from the symmetry of the local environment. However, in many cases it is not so easy to find these directions, especially in the case of distorted mixed ligand environment. One of the possibilities to solve this problem is the use of the crystal field gradient tensor. The calculation details can be found elsewhere [39]. The matrices build from the eigenvectors of the crystal field gradient tensors are the transformation matrices $\boldsymbol{\nu}$ in Eq. (4). The sign of the greatest in absolute magnitude eigenvalue gives information about the type of distortion. If this value is positive the corresponding distortion is axial compression, while the negative value corresponds to axial elongation of the local octahedron. As a consequence, the sign of the axial Δ parameter of the local $\mathbf{\Delta}$ tensor can be predicted (see discussion after Eq. (4)).

Depending on the system under investigation the general Hamiltonian can be constructed from the interactions mentioned above. The values of the magnetization and the magnetic susceptibility for an arbitrary direction of the applied magnetic field can be calculated as

$$M(\vartheta, \varphi) = N_A k_B T \frac{\partial}{\partial H(\vartheta, \varphi)} \{\ln Z[H(\vartheta, \varphi)]\}, \tag{8}$$

$$\chi(\vartheta, \varphi) = \frac{M(\vartheta, \phi)}{H(\vartheta, \phi)}. \tag{9}$$

Z is the partition function and k_B and N_A are the Boltzmann's constant and Avogadro's number, respectively. The powder averaged magnetic susceptibility can be calculated as $\chi_{av} = (\chi_x + \chi_y + \chi_z)/3$, whereas for the calculation of magnetization the averaging over all possible orientations of the external magnetic field must be performed. For the exchange coupled systems this averaging procedure, in general, is time-consuming due to the large size of the matrices to be diagonalized (for polynuclear complex containing n Co(II) ions the size of corresponding matrices is $12^n \times 12^n$) and some simplification is required. The relatively strong spin–orbit coupling results in a ground state doublet on each cobalt ion. This Kramers doublet is well separated from the excited levels. The effect of the low-symmetry field does not change this conclusion (we neglect the case of strong positive Δ, where the orbital angular momentum is completely quenched). As a result, at low temperatures only these ground state Kramers doublets of each cobalt ion are thermally populated. Both the exchange coupling and the Zeeman interaction are much smaller than the energy separation between the ground state doublet and the excited levels and can be regarded as a perturbation operating within the restricted space of the direct product of the Kramers doublets. The effect of the excited levels on the magnetic properties can be taken into account by the second-order perturbation theory. The magnetization at low temperatures can be easily simulated since instead of $12^n \times 12^n$ matrices one deals with $2^n \times 2^n$ matrices.

The presented above approach allows one to fully describe the magnetic properties of the exchange coupled dimeric and trimeric complexes. However, for polynuclear system the size of matrices to be diagonalized for the calculation of the magnetic susceptibility grows rapidly. The task becomes intractable. An attempt to solve this problem can be found in Ref. [40]. The approach is based on the effective-spin-1/2 formalism and the temperature dependent Landé factor. However, the anisotropy of the exchange interaction between effective spins is not taken into account. This anisotropy depends on the value of the low symmetry crystal field parameter Δ as well as on the angle between the local symmetry axes of the interacting ions and strongly affects the magnetic properties of exchange coupled Co(II) complexes at low temperature.

2.2. Magnetic circular dichroism

A general formula for the analysis of MCD spectra requires the calculation of the difference between molar extinction coefficients for the left and right circularly polarized light, i.e., $\Delta\varepsilon = \varepsilon_L - \varepsilon_R$. In the case of mononuclear complexes with the orbitally degenerate ground-state, MCD saturation behavior depends on the polarization of the corresponding transitions and can be simulated as [41]

$$\Delta\varepsilon(\vartheta, \varphi) \propto M_{xy}^{eff} \cos\vartheta \langle L^z\rangle_T + M_{xz}^{eff} \sin\vartheta \sin\varphi \langle L^y\rangle_T + M_{yz}^{eff} \sin\vartheta \cos\varphi \langle L^x\rangle_T, \tag{10}$$

where M_{ij}^{eff} is a combination of matrix elements of i-th and j-th components of electric dipole operator and $\langle L^k\rangle_T$ is thermally averaged component of the orbital angular momentum within the ground state:

$$\langle L^k\rangle_T = \frac{1}{Z} \sum_g \langle g|L^k|g\rangle \exp\left(\frac{-E_g}{k_B T}\right), \quad k = x, y, z \tag{11}$$

and ϑ and φ describe the orientation of the magnetic field with respect to the molecule-fixed coordinate system. To obtain the signal from the randomly oriented molecules Eq. (10) is integrated over all magnetic field orientations.

For a mononuclear Co(II) complex in the distorted octahedral environment Eq. (10) can be simplified. The relatively strong spin–orbit coupling results in a Kramers doublet well separated from the excited levels. At low enough temperatures (where data for saturation magnetization curves are usually collected) only this ground state doublet is thermally populated and the influence of the excited levels can be neglected. If distortion from the octahedral environment is small, this ground state Kramers doublet possesses an isotropic g-value and Eq. (10) can be rewritten as

$$\Delta\varepsilon = A_{sat} \tanh\left(\frac{g\mu_B H}{2k_B T}\right) \tag{12}$$

with $g = (5/3)g_0 + \kappa$. The optical transitions of all polarizations should contribute to the MCD spectrum and the saturation magnetization curves recorded at different wavelengths must be similar and overlapping when plotted as a function of H/T.

If distortion from the octahedral environment is very strong and Δ-value is negative, the ground state Kramers doublet becomes strongly anisotropic. The corresponding g-values are $g_{||} = 3(g_0 + \kappa)$, $g_\perp = 0$ and only xy-polarized optical transitions contribute to the MCD spectrum. For very strong positive Δ-values the orbital angular momentum disappears. High-spin Co(II) ion can be treated as a $S = 3/2$ spin with strong magnetic anisotropy. The MCD signal appears as a result of spin–orbit admixture of some states to the ground and/or excited states [41,42]. The signal behavior depends strongly on the polarization of the corresponding transitions and can be simulated with the use of Eqs. (10) and (11) where instead of the orbital angular momentum the components of spin are used. For monomuclear Co(II) complexes in pseudo tetrahedral environment the orbital angular momentum is completely quenched and the situation is similar to the case of octahedrally coordinated Co(II) with strong positive Δ.

Analysis of MCD behavior of the exchange coupled systems is a complicated topic. If the exchange parameter is relatively big, the energy spectrum of the system represents the groups of levels (multiplets) well separated from each other and at low temperatures ($k_B T \ll J_{ex}$) Eqs. (10) and (11) can be applied to the ground state multiplet and, as a consequence, to the whole system. In the

case of weak exchange-coupled systems Eq. (10) is not valid. In this case, for each transition only the contribution from a single ion to $\langle L^k \rangle_T$ is needed and, in general, this could lead to the situation where transitions of the same polarization but localized at different centers possess different magnetization curves [43]. In terms of Eq. (10) it means that different thermally populated multiplets have different M_{ij}^{eff}-values. Typical values of J_{ex}-parameter in the exchange coupled Co(II) complexes are about several wave numbers, however, in the case of binuclear cobalt systems the situation is favorable. At low temperatures each Co(II) ion can be treated as a pseudo-spin-1/2 system. Exchange interaction couples these pseudo-spins to the states with the total angular momentum $J = 0$ and 1. Both states are thermally accessible, however, state with $J = 0$ is a non-magnetic one and does not contribute to the MCD C-term. So, Eq. (10) can be applied to the $J = 1$ state and to the whole dimer. Due to the anisotropy of the exchange interaction that operates within the restricted space of the direct product of the ground state Kramers doublets, the $J = 1$ state is split and it affects the MCD saturation behavior. Since this anisotropy strongly depends on the magnitude and the sign of Δ parameter (see for example Fig. 6 in Ref. [44]), analysis of MCD behavior gives not only the value of the exchange parameter but information about the type and the strength of the distortion of the local environment as well.

In the case of exchange coupled Co(II) trimers three pseudo-spins-1/2 are coupled to the states with the total angular momentum $J = 1/2$, 1/2 and 3/2. All states result in MCD C-term and, in general, Eq. (10) cannot be used. However, in some cases Eq. (10) still gives relatively good simulation of the experimental MCD saturation behavior.

3. Examples

3.1. Monomers $Co(tu)_4(NO_3)_2{\cdot}H_2O$ and $Co(pybzim)_2Cl_2$

Here we present one example each for tetrahedral and octahedral coordination, based on susceptibility, magnetization and MCD measurements [45].

3.1.1. $Co(tu)_4(NO_3)_2{\cdot}H_2O$ (**1**): tetrakis(thiourea)dinitrate monohydrate as an example of Co(II) in tetrahedral coordination

The crystal structure is described in Ref. [46], see Fig. 2. The Co(II) is fourfold coordinated by thiourea groups. The coordinating tetrahedron is strongly distorted.

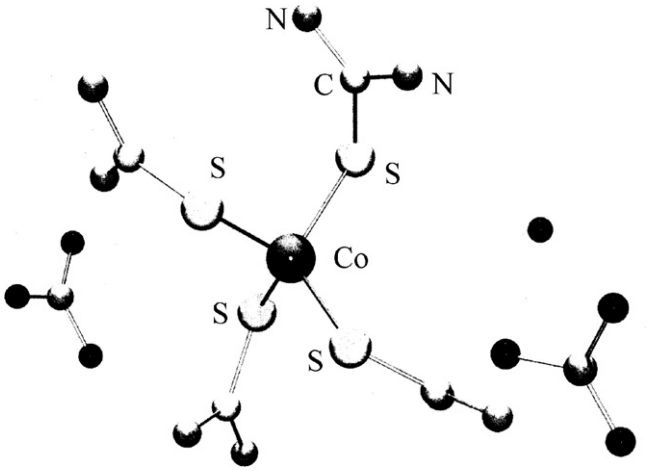

Fig. 2. Molecular structure of complex (**1**).

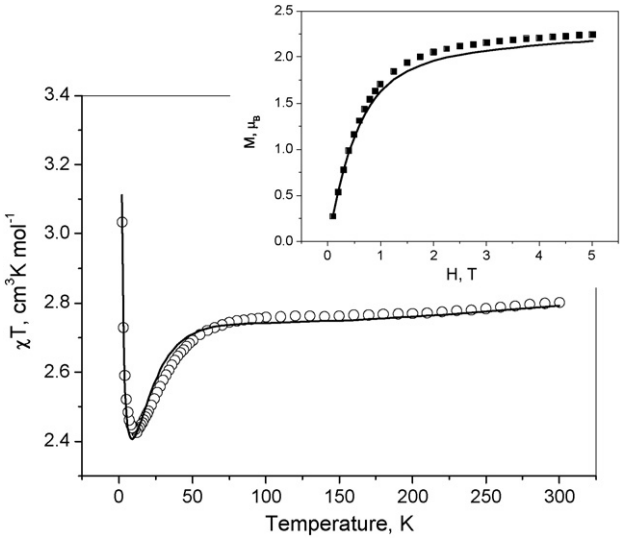

Fig. 3. Experimental magnetic properties of complex (**1**). Inset is the magnetization vs. field at 2 K. Theoretical curves are calculated at $D = -30\,cm^{-1}$, $g_{||} = 2.7$, $g_{\perp} = 2.16$, $zJ = 0.11\,cm^{-1}$, $\chi_{TIP} = 0.0005\,cm^3\,mol^{-1}$.

Low temperature magnetic properties (see Fig. 3) indicate some intermolecular interaction. This intermolecular interaction was included into consideration in the mean-field approximation: $\mathbf{H}_{int} = -zJ(\mathbf{S}_x\langle S_x\rangle + \mathbf{S}_y\langle S_y\rangle + \mathbf{S}_z\langle S_z\rangle)$, where $\langle S_i\rangle$ is the mean value of i-th component of the spin operator and z is the number of nearest neighbors. This intermolecular interaction was added to the Hamiltonian Eq. (6). The procedure is the following: the self-consistent set of equations for the averaged values of S_i ($i = x, y, z$) is solved for an arbitrary magnitude and direction of the external magnetic field. At the next step, the magnetization along the direction of the applied magnetic field is found. Magnetic susceptibility at some given value and direction of the external magnetic field is calculated using Eq. (9). To obtain the powder averaged values of $M(H)$ and $\chi(T)$, integration over all possible orientation of the applied magnetic field is performed. Although the symmetry of the complex is very low (C_2), the axial model results in a good explanation of the magnetic behavior (Fig. 3). The D-parameter obtained, equal to $-30\,cm^{-1}$ looks rather large for the tetrahedrally coordinated

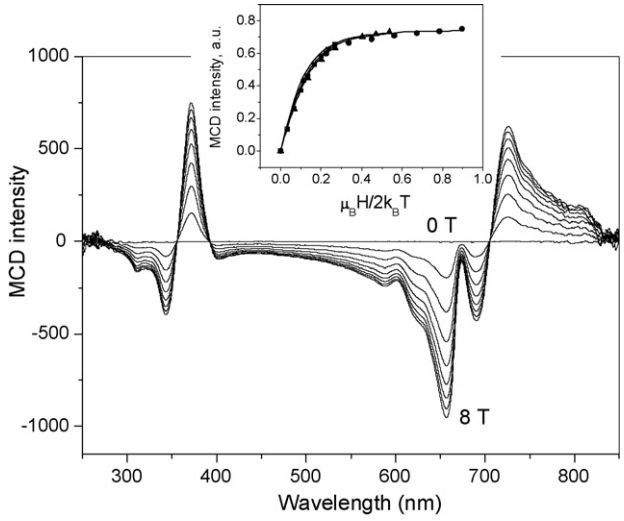

Fig. 4. Experimental MCD spectrum of complex (**1**) at 10 K. Inset is the magnetization curves at 657 nm, theoretical curves are calculated at the assumption of xy-polarization of optical transitions.

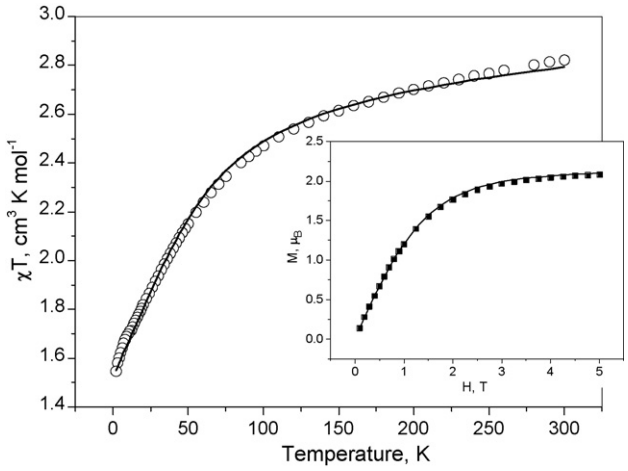

Fig. 5. Experimental magnetic properties of complex (**2**). Inset is the magnetization vs. field at 2 K. Theoretical curves are calculated at $D = 51.2\ cm^{-1}$, $g_{||} = 2.62$, $g_{\perp} = 2.29$, $\chi_{TIP} = 0.0005\ cm^3\ mol^{-1}$.

cobalt(II), however, there are some examples with even greater values of the *D*-parameter [5].

The MCD spectrum of $Co(tu)_4(NO_3)_2{\cdot}H_2O$ complex is presented in Fig. 4. The saturation behavior can be also explained in the axial model. However, for detailed analysis of signal behavior and polarization of corresponding optical transitions, the rhombic distortions must be taken into consideration.

One reason for the relatively large *D*-parameter value of the tetrahedrally coordinated Co(II) can be the presence of an intercluster interaction. This interaction influences the magnetic properties at low temperature and prevents the accurate determination of axial ZFS parameter. However, MCD studies confirm the *D*-value, obtained from the magnetic investigations.

3.1.2. *Co(pybzim)$_2$Cl$_2$ (**2**): dichloro-di-(2,2′-pyridine-benzimidazol)cobalt(II) as an example of Co(II) in distorted octahedral coordination*

Co(II) is octahedrally coordinated by four nitrogen atoms of the two bidendate ligands and two coordinated chlorine ions [47]. The magnetic properties were analyzed with the use of Hamiltonian, Eq. (6), in the axial model. The values of the best-fit parameters are typical for the high-spin Co(II) in the octahedral environment (see Fig. 5). Although the powder averaged magnetic properties are well explained in the axial model, for MCD saturation behavior the situation is less satisfactory. The saturation behavior at 487 nm can

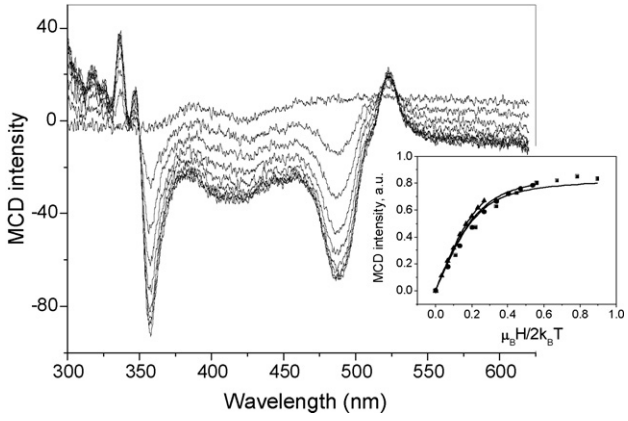

Fig. 6. Experimental MCD spectrum of complex (**2**) at 3 K. Inset is the magnetization curves at 487 nm, theoretical curves are calculated at the assumption $M_{xy}^{eff} = 0$.

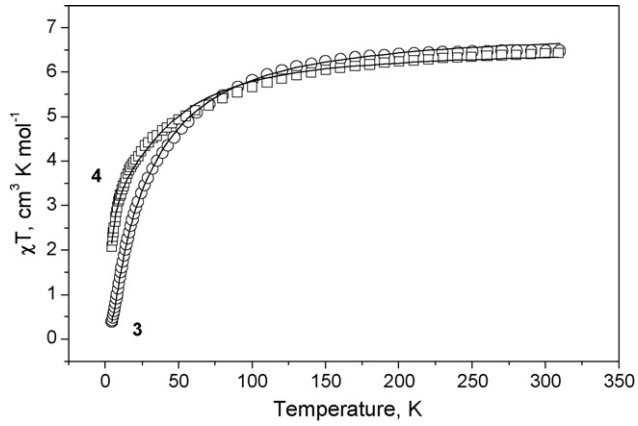

Fig. 7. Experimental magnetic properties of complexes (**3**) (circles) and (**4**) (squares). Theoretical curves are calculated at $J_{ex} = -3.6\ cm^{-1}$, $D = 30\ cm^{-1}$, $g_{||} = 3.0$, $g_{\perp} = 2.6$ (**3**) and $J_{ex} = -0.7\ cm^{-1}$, $D = 45\ cm^{-1}$, $g_{||} = 2.9$, $g_{\perp} = 2.5$ (**4**).

be reproduced with the assumption of polarization in the plane of the local *z*-axis (Fig. 6), however, the signal behavior at 357 nm can not be explained in the axial model. Some low symmetry distortion must be taken into consideration.

3.2. Dimers

Here we present some results of our investigations on five Co(II) dimers (**3–7**) but their electronic behavior is different.

3.2.1. *[Co$_2$(μ-OAc)$_2$(μ-AA)(urea)(tmen)$_2$][OTf] (**3**), [Co$_2$(μ-H$_2$O)(μ-OAc)$_2$(OAc)$_2$(tmen)$_2$] (**4**): spin-only model and antiferromagnetic coupling*

For these two complexes only magnetic susceptibility data were used. The crystal structure of (**3**) is presented in Ref. [48], and for (**4**) in Ref. [49]. Both complexes are bridged by two acetate groups and additionally in the first case by an acetatohydroxamate group, while in the second case by water [48–50].

The coordination about each Co(II) atom in both complexes is a distorted octahedron. However, the symmetry is very low and the orbital angular momentum is assumed to be completely quenched. In general, three different principal values of local **g**- and ***D***-tensors must be taken into account for the comprehensive description of the regarded compounds, however, such detailed consideration is overcomplicated for the explanation of powder averaged magnetic data. The analysis was based on the assumption of strong local anisotropy of Co centers in the axial model. The angle between the local z_i axes was found from the symmetry point of view. For both complexes the spin-only model gives a good interpretation of the magnetic behavior. The calculated values of the axial ZFS parameter are typical for octahedrally coordinated high-spin Co(II) ions: $30\ cm^{-1}$ for [Co$_2$(μ-OAc)$_2$(μ-AA)(urea)(tmen)$_2$][OTf] complex and $45\ cm^{-1}$ for [Co$_2$(μ-H$_2$O)(μ-OAc)$_2$(OAc)$_2$(tmen)$_2$] one. In both systems the exchange interaction is antiferromagnetic, however, since the bridging water in this case obviously does not provide a good pathway for superexchange, this interaction in the corresponding complex is weaker ($-0.7\ cm^{-1}$ as compared to $-3.6\ cm^{-1}$). The χT vs. *T* dependences for both complexes are presented in Fig. 7.

3.2.2. *[Co$_2$(μ-OAc)$_3$(urea)(tmen)$_2$][OTf] (**5**): spin–orbit interaction and ferromagnetic coupling*

The next complex studied [Co$_2$(μ-OAc)$_3$(urea)(tmen)$_2$][OTf] represents an example of ferromagnetically coupled Co(II) dimer. Compared to compound (**3**), the bridging hydroxamate group is substituted by an acetate group in (**5**). In order to compare, in com-

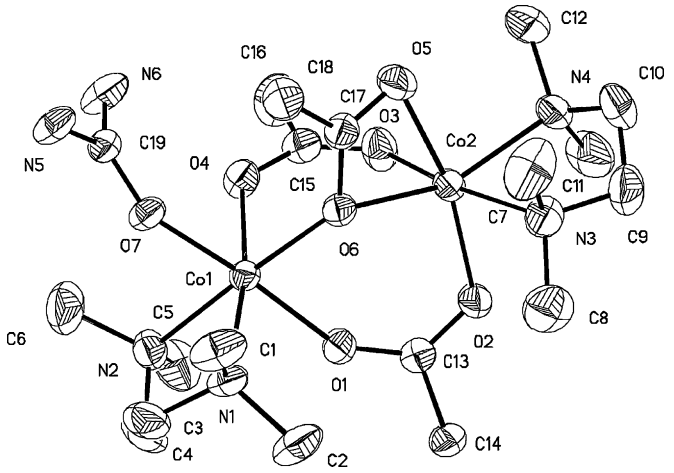

Fig. 8. Molecular structure of complex (**5**). Figure was reproduced from Ref. [35], with permission of the copyright holders.

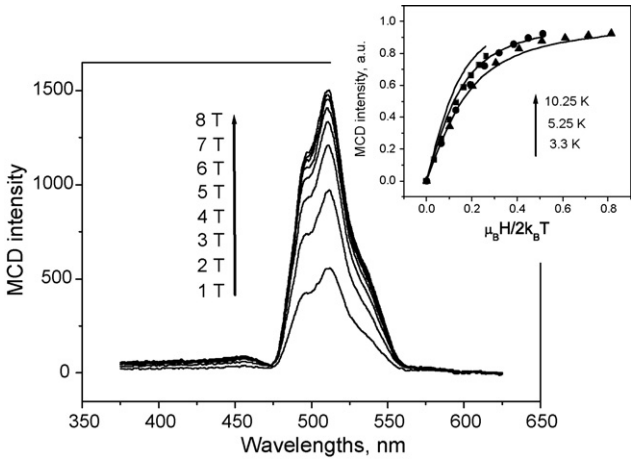

Fig. 10. Experimental MCD spectrum of complex (**5**) at 3.3 K. Inset is the magnetization curves at both 495 and 510 nm, theoretical curves are calculated at the assumption $M_{xy}^{eff} = M_{xz}^{eff} = M_{yz}^{eff}$.

pound (**4**) the bridging water substitutes the bridging oxygen of the hydroxamate group in compound (**3**) and the acetate group in compound (**5**).

The crystal structure is shown in Fig. 8 [35]. Each cobalt ion is octahedrally coordinated, but the site symmetry is lower because of some distortions in the environment. The directions of the local coordinate axes which coincide with the main axes of the local **Δ**-tensors were found on the basis of the symmetry of the nearest environment (the details are presented elsewhere [35]). From the analysis of magnetic behavior the values of the key parameters of the complex were obtained (Fig. 9). The ferromagnetic exchange interaction results in the $J = 1$ ground state of the complex. This ground state possesses an effective g-factor of about 4.73, which large value is the result of the strong orbital contribution to the magnetic behavior of the cobalt dimer and cannot be explained in the spin-only model. The magnetic behavior of the cobalt dimer is explained by the interplay of two processes: the thermal population of the excited levels that are less magnetic than the ground one and the strong temperature-independent part of the magnetic susceptibility. When the temperature is low enough and the thermal population of the excited levels is small, the latter process dominates, and the effective magnetic moment increases with increasing temperature. At some value of temperature, the population of the levels with smaller g values becomes significant, and further temperature growth leads to the decrease of the effective magnetic moment.

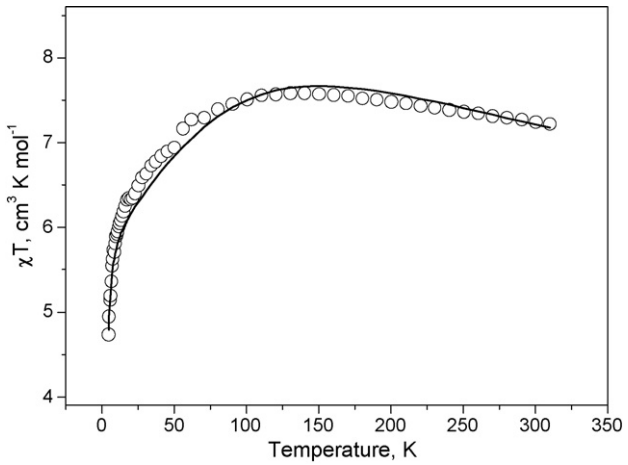

Fig. 9. Experimental magnetic properties of complex (**5**). Theoretical curves are calculated at $J_{ex} = 18.0\,cm^{-1}$, $\kappa = 0.7$, $\Delta = 80\,cm^{-1}$, $E = 10\,cm^{-1}$.

The experimental MCD spectrum in the visible range (see Fig. 10) consists of two intense bands at 495 and 510 nm and is dominated by temperature-dependent contributions [35]. The intensity behavior at both wavelengths is similar and after normalization, curves at both wavelengths coincide. The corresponding saturation curves are presented in the inset to Fig. 10. The initial slope of these saturation curves clearly demonstrates that the exchange interaction in the complex studied is ferromagnetic and the ground state is the magnetic one. Since the value of the Δ-parameter is relatively small, the transitions of all polarizations should contribute to the MCD spectrum. The theoretical curves were constructed with the use of Eq. (10) with the assumption that the contribution of all polarizations is equivalent. There is a reasonable agreement between the experimental data and theoretical curves confirming the applicability of the model presented for the theoretical explanation of the magneto-optical behavior of the cobalt dimer investigated.

*3.2.3. $Co_2[(\mu\text{-}H_2O)(\mu\text{-}OAc_{Cl})_2(H_2O)_2(OAc_{Cl})_2\cdot 1.5C_4H_8O_2]\cdot C_4H_8O_2$ (**6**) and $Co_2[(\mu\text{-}H_2O)(\mu\text{-}OAc_{Cl})_2(H_2O)_4(OAc_{Cl})_2]\cdot H_2O$ (**7**): dimers with spin–orbit interaction and antiferromagnetic coupling*

The main peculiarity of both complexes [51] is the presence of water molecules both as a bridging and terminal ligands. Bridging water was also present in the dimer (**4**). In Fig. 11 the crystal structure of (**6**) is presented. Each Co(II) is coordinated by one bridging water, two bridging trichloroacetate groups, one non-bridging trichloroacetate group and one non-bridging water. Two dimers are bridged by one dioxane group, the external Co(II) ion is bonded to one dioxane molecule. In fact one could speak of linear tetramers, but magnetically two slightly interacting dimers are present. The refinement of the crystal structure of (**7**) ended in an insufficient state [52] but it is evident that the central molecule groups of (**6**) and (**7**) are directly comparable.

The directions of the local coordinate axes were found by diagonalization of the crystal field gradient tensor. That the oxygen from the water molecule is less charged than the oxygen from other ligands was taken into account. A simultaneous fit of both χT and magnetization experimental data allows one to obtain the main parameters of the complexes with results shown in Figs. 12 and 13. The best-fit parameters for both complexes look similar. The exchange interaction is antiferromagnetic. The values

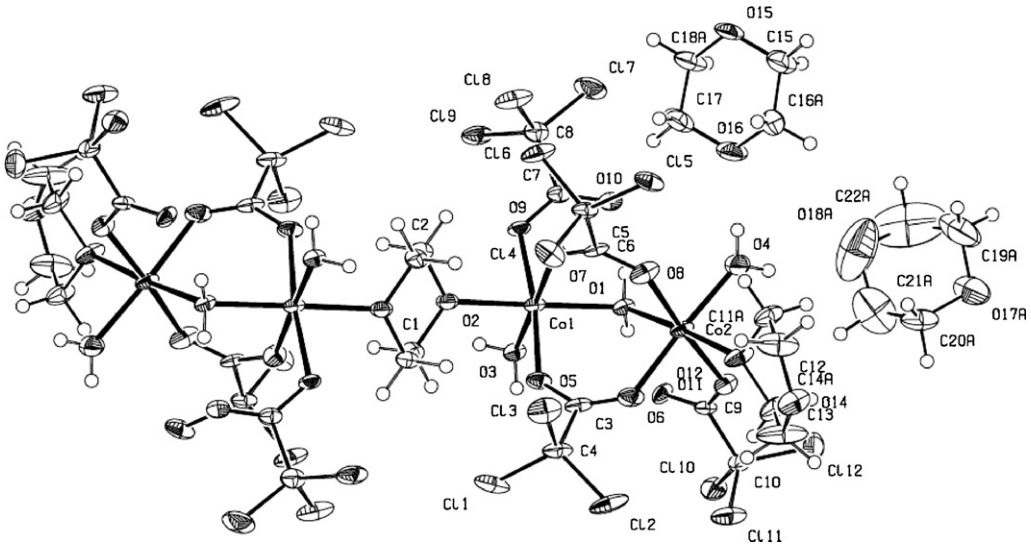

Fig. 11. Molecular structure of complex (**6**).

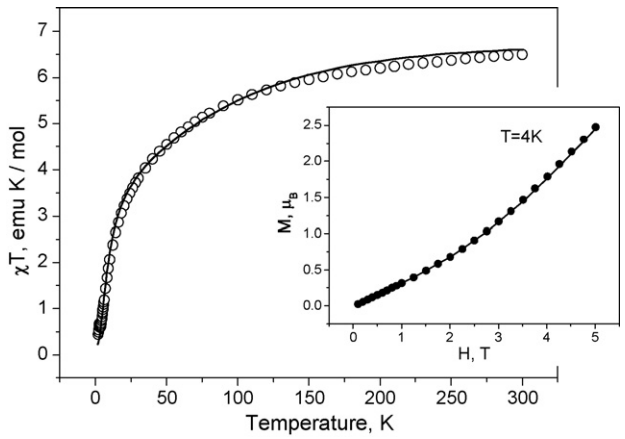

Fig. 12. Experimental magnetic properties of (**6**). Inset is the magnetization vs. field at 4 K. Theoretical curves are calculated at $J_{ex} = -2.09\,cm^{-1}$, $\kappa_1 = \kappa_2 = 0.97$, $\Delta_1 = -1196\,cm^{-1}$, $\Delta_2 = 476\,cm^{-1}$.

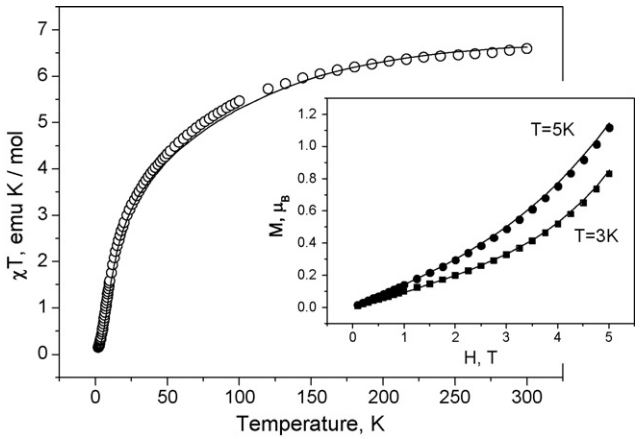

Fig. 13. Experimental magnetic properties of (**7**). Inset is the magnetization vs. field at 3 and 5 K. Theoretical curves are calculated at $J_{ex} = -2.91\,cm^{-1}$, $\kappa_1 = \kappa_2 = 0.97$, $\Delta_1 = -720\,cm^{-1}$, $\Delta_2 = 473\,cm^{-1}$.

of the orbital reduction factor are very close to the weak field limit ($\kappa = 1$) that is caused by the presence of water molecules in the nearest environment. The values of Δ_i-parameters indicate that the distortions around one of Co ions in the dimer can be described as an axial elongation while for another one an axial compression takes place. This conclusion agrees well with the analysis based on the diagonalization of the crystal field gradient tensor. In (**7**) the axial compression (negative Δ-value) is smaller than in (**6**), which can be explained by the presence of the greater number of water molecules in the local environment of the corresponding ion.

The experimental MCD spectra for both complexes are similar and consist of one intense broad band at about 515 nm (Figs. 14 and 15). The saturation magnetization curves differ from those for $[Co_2(\mu\text{-}OAc)_3(urea)(tmen)_2][OTf]$ complex. From the analysis of these curves one immediately concludes that the ground state of the complexes (**6**) and (**7**) is non-magnetic, however, the magnetic excited states are close in energy to the ground one and the exchange interaction is antiferromagnetic and small. The theoretical simulation of the magnetization curves shows that the corresponding optical transitions are mainly polarized in the plane formed by the local z_i axes. The strong dependence of the signal behavior on the polarization of the corresponding transitions is typical for strongly distorted systems and confirms the large values of Δ_i-parameters.

The MCD investigation of the antiferromagnetically coupled Co(II) dimer was presented in Ref. [19]. The theoretical analysis was based on the assumption that the signal comes from the groups of singlets and doublets that are thermally populated. This description is correct when the external magnetic field is applied along *z*-direction (the corresponding optical transitions are *xy*-polarized). However, when the magnetic field is applied perpendicular to the *z*-direction, the behavior of the lowest levels is more complicated than the behavior of two singlets and one doublet. In general, for such cases Eq. (10) must be used.

3.3. Linear trimers

3.3.1. $[Co_3(\mu\text{-}H_2O)_2(\mu\text{-}OAc_F)_4(OAc_F)_2(H_2O)_2(C_4H_8O_2)]\cdot 2C_4H_8O_2$ (**8**): spin–orbit coupling and weak antiferromagnetic exchange interaction

The linear trimer (**8**) is composed of three tetragonally distorted Co(II) centers bridged by four trifluoroacetate groups and two bridging water molecules [53] (see Fig. 16).

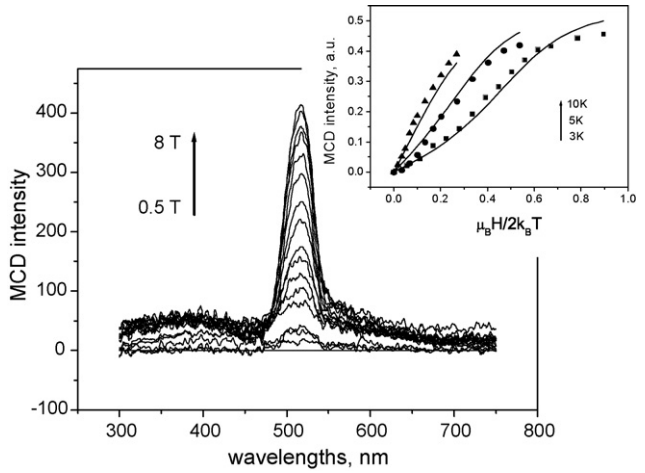

Fig. 14. Experimental MCD spectrum of complex (**6**) at 3 K. Inset is the magnetization curves at 517 nm, theoretical curves are calculated at the assumption $M_{xy}^{eff} = M_{yz}^{eff} = 0$.

From the structural analysis of the compound studied, one can see that C_4 axes of terminal ions are parallel to each other and not parallel to the C_4 one of the central ion. These C_4 axes were assigned as local z_i ones. Since the exchange interaction via the water molecule is expected to be small, the experimental magnetic data were split in two subsets: for temperatures lower and higher than 50 K. The low temperature region was analyzed with the use of the second-order perturbation theory while for high temperatures any exchange interaction was neglected and the studied trimer was regarded as three non-interacting Co ions. In the final step, the best-fit parameters obtained (see caption to Fig. 17) were used for the calculation of the magnetic behavior of the trimer in the framework of the general model (1728 × 1728 matrices) in the whole temperature range. The magnetic exchange is antiferromagnetic and small. The values of the orbital reduction factor are in the middle between the weak and strong field limits. Best-fit values of the low-symmetry component of the crystal field indicate that for the terminal ions the distortions from the octahedral environments are stronger than those for the central one which is in a good agreement with the structural data.

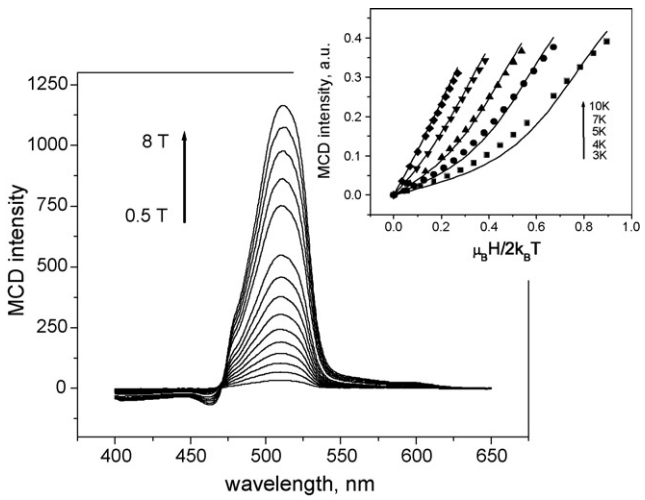

Fig. 15. Experimental MCD spectrum of complex (**7**) at 3 K. Inset is the magnetization curves at 512 nm, theoretical curves are calculated at the assumption $M_{xy}^{eff} = M_{yz}^{eff} = 0$.

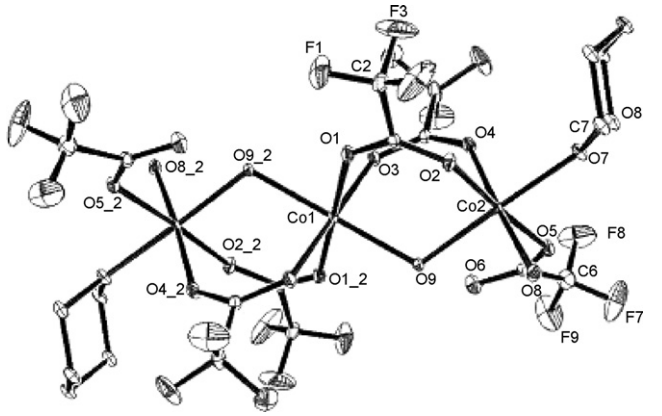

Fig. 16. Structure of (**8**). Figure was reproduced from ref. [53], with permission of the copyright holders.

3.3.2. *[$Co_3(\mu$-$OAc_F)_4(\mu$-$AA)_2(tmen)_2$] (**9**), [$Co_3(\mu$-$OAc_F)_4(\mu$-$BA)_2(tmen)_2$] (**10**): spin–orbit coupling and antiferromagnetic exchange interaction*

Magneto-optical studies of new trinuclear complexes (**9**) and (**10**) have been published in Ref. [39]. In each structure, the Co(II) ions have distorted octahedral coordination and are triply bridged by one hydroxamate (AA) or benzohydroxamate (BA) group, respectively, and two trifluoroacetate group bridges (Fig. 18).

The directions of the local coordinate axes were found by the diagonalization of the crystal field gradient tensor. A simultaneous fit of both χT and magnetization experimental data allows one to obtain the main parameters of the complexes (see captions to Figs. 19 and 20). For both complexes the exchange interaction is antiferromagnetic. The κ values are typical for this type of compounds.

The experimental MCD spectra of both trimers, see Figs. 21 and 22, are similar and dominated by temperature-dependent contributions. The strong signal at 324 nm corresponds to ligand–metal charge transfer, whereas bands at 495 and 510 nm are typical for d–d transitions. Signals recorded at different wavelengths demonstrate different saturation behavior (insets to Figs. 21 and 22) which is typical for the complexes where orbital

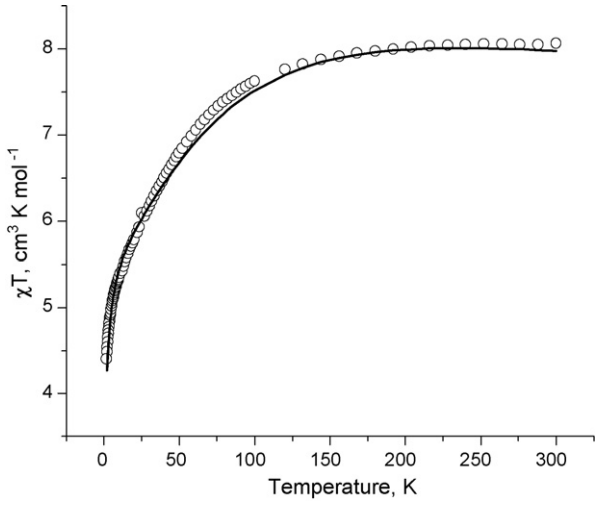

Fig. 17. Experimental magnetic properties of complex (**8**). Theoretical curve is calculated at $J_{ex} = -0.4\,cm^{-1}$, $\kappa_1 = 0.77$, $\kappa_2 = \kappa_3 = 0.72$, $\Delta_1 = -970\,cm^{-1}$, $\Delta_2 = \Delta_3 = -1160\,cm^{-1}$. Figure was reproduced from Ref. [53], with permission of the copyright holders.

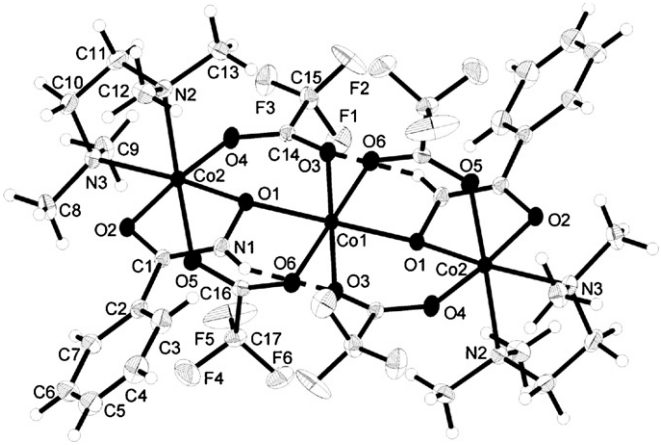

Fig. 18. Molecular structure of complex (**10**). Figure was reproduced from Ref. [39], with permission of the copyright holders.

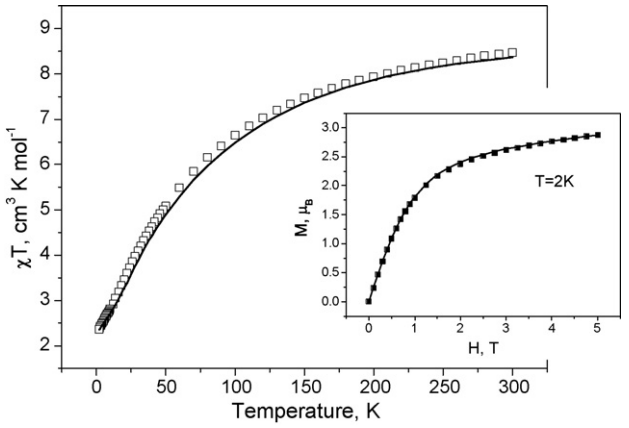

Fig. 19. Experimental magnetic properties of complex (**9**). Inset is the magnetization vs. field at 2 K. Theoretical curves are calculated at $J_{ex} = -6.4\,cm^{-1}$, $\kappa_1 = 0.92$, $\kappa_2 = \kappa_3 = 0.9$, $\Delta_1 = 645\,cm^{-1}$, $\Delta_2 = \Delta_3 = -642\,cm^{-1}$.

angular momentum is partially or completely quenched. This can be regarded as a confirmation of relatively large Δ-values. Since the ground state of Co trimer is the magnetic one ($J = 1/2$ in the case of antiferromagnetic exchange interaction), at first glance the saturation behavior looks similar to that of the ferromagnetically

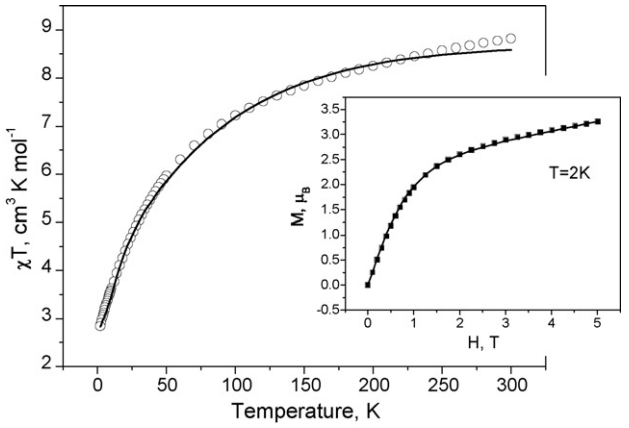

Fig. 20. Experimental magnetic properties of complex (**10**). Inset is the magnetization vs. field at 2 K. Theoretical curves are calculated at $J_{ex} = -3.1\,cm^{-1}$, $\kappa_1 = 0.82$, $\kappa_2 = \kappa_3 = 0.88$, $\Delta_1 = 372\,cm^{-1}$, $\Delta_2 = \Delta_3 = -775\,cm^{-1}$.

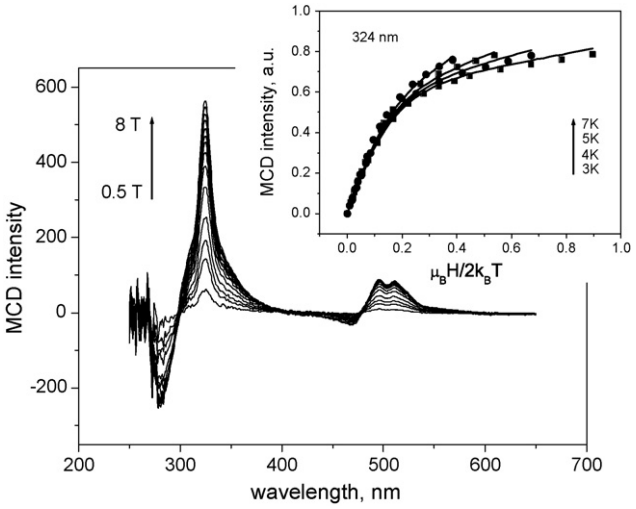

Fig. 21. Experimental MCD spectrum of complex (**9**) at 3 K. Inset is the magnetization curves at 324 nm, theoretical curves are calculated at the assumption $M_{xy}^{eff} = 0$, $M_{xz}^{eff} = M_{yz}^{eff}$.

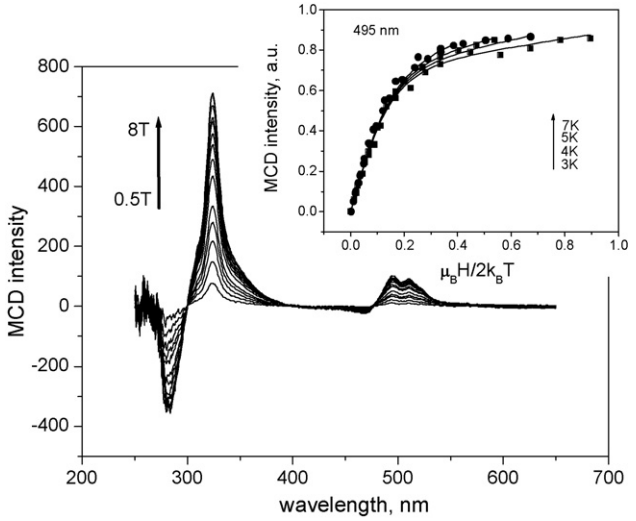

Fig. 22. Experimental MCD spectrum of complex (**10**) at 3 K. Inset is the magnetization curves at 495 nm, theoretical curves are calculated at the assumption $M_{xz}^{eff} = M_{yz}^{eff} = 0$.

coupled $[Co_2(\mu\text{-}OAc)_3(urea)(tmen)_2][OTf]$ (**5**) dimer. However, the temperature dependence of the signal is stronger than in the dimeric complex indicating that there are excited magnetic levels close in energy to the ground one. In the CoBA-trimer the exchange interaction is weaker, the excited levels are closer and, as a consequence, the temperature dependence of signal saturation behavior is more pronounced.

4. Concluding remarks

In this contribution the investigation of complexes containing mononuclear and exchange coupled high-spin Co(II) ions was presented. Different experimental techniques such as magnetic susceptibility in a wide temperature range, magnetization vs. magnetic field at low temperatures and MCD were used. Theoretical analysis was performed on the basis of different models. In many cases the ZFS approach is not applicable to the explanation of the magneto-optical behavior of the complexes,

containing high-spin Co(II) in the octahedral environment, and orbital angular momentum must be included into consideration.

The ZFS is also commonly accepted as a coordination number indicator. But, there is a remarkable overlap between particular intervals corresponding to different coordinations. Some rare cases are reported with a high value of ZFS which lies far outside the typical intervals, namely $D \approx -100\,cm^{-1}$ for one distorted tetrahedrally coordinated Co(II) ion [5]. The value of ZFS $D = -30\,cm^{-1}$ found in this work for the tetrahedrally coordinated $Co(tu)_4(NO_3)_2{\cdot}H_2O$ is on the one hand much lower, but, if compared to the typical D values, still high. In both complexes the tetrahedrally distorted Co(II) ions are directly bonded to sulfur ligands. In general, one can conclude that the kind of ligands, the covalency of the bond, and the orientation of the ligands will influence the D value.

The exchange interactions, obtained for the series of studied dimers and trimers are weak and antiferromagnetic. For water-bridged complexes this exchange is weaker than for other ones since this kind of bridge does not provide a good pathway for superexchange. The only exception is the binuclear complex $[Co_2(\mu\text{-OAc})_3(urea)(tmen)_2][OTf]$ (**5**) for which a positive exchange constant $J_{ex} = 18\,cm^{-1}$ was obtained. The major difference between the antiferromagnetically coupled complex (**3**) and ferromagnetically coupled complex (**5**) is the substitution of the hydroxamate bridge in (**3**) by an acetato bridge in (**5**).

Magnetic, magnetization and MCD investigations accompanied by theoretical calculations complement each other. Although the magnetization curves from field dependent measurements and from MCD experiments look similar at first glance, their temperature and field dependence is different because the MCD signal depends both on the ground and excited states and, as a consequence, on the polarization of the corresponding optical transitions. Even if this polarization is unknown from the experiment, MCD curves provide some additional information and allow one to determine independently and/or to confirm the key parameters of the system. For example, low symmetry distortion of the ligand environment has no significant effect on the powder averaged magnetic properties while the MCD saturation behavior is very sensitive to this kind of distortion. One more point is that MCD saturation curves reflect only the magnetic behavior of the complex, responsible for the corresponding optical transition, while for magnetic measurements it is very difficult to separate the contribution from some magnetic impurities. It is therefore highly recommended to collect as much as possible data from the different methods in order to deal with such non-trivial problem like high-spin Co(II).

Acknowledgements

Financial support by German Science Foundation via the projects Ha 782/65 and Ha 782/85 (Priority Project 'Molekularer Magnetismus') is acknowledged. We acknowledge long lasting cooperation with Professor David Brown and cooperation with Professor V. Calvo-Perez. We thank J. Pelikan for collecting the MCD spectra of the two monomers. Fruitful discussions with Professors R. Boca and M. Zeppezauer are thankfully acknowledged.

References

[1] O. Kahn, Molecular Magnetism, VCH Publishers, New York, 1993.
[2] E.A. Boudreaux, L.N. Mulay, Theory and Applications of Molecular Paramagnetism, John Willey & Sons, New York, 1976.
[3] R. Boča, Theoretical Foundation of Molecular Magnetism, Elsevier, Amsterdam, 1999.
[4] (a) K. Krzystek, A. Ozarowski, J. Telser, Coord. Chem. Rev. 250 (2006) 2308; (b) M.W. Makinen, M.B. Yim, Proc. Natl. Acad. Sci. U.S.A. 78 (1981) 6221.
[5] K. Fukui, H. Ohya-Nishiguchi, N. Hirota, Bull. Chem. Soc. Jpn. 64 (1991) 1205.
[6] R. Boča, L. Dlhan, W. Linert, H. Ehrenberg, H. Fuess, W. Haase, Chem. Phys. Lett. 307 (1999) 359.
[7] L. Banci, A. Bencini, C. Benelli, D. Gatteschi, C. Zanchini, Struct. Bond. 52 (1982) 37.
[8] J.A. Larrabee, C.M. Alessi, E.T. Asiedu, J.O. Cook, K.R. Hoerning, L.J. Klinger, G.S. Okin, S.G. Santeee, T.L. Volkert, J. Am. Chem. Soc. 119 (1997) 4182.
[9] J.A. Larrabee, C.H. Leung, R.L. Moore, T. Thamrong-nawasawat, B.S.H. Wessler, J. Am. Chem. Soc. 126 (2004) 12316.
[10] J.S. Taylor, C.Y. Lau, M.L. Applebury, J.E. Coleman, J. Biol. Chem. 248 (1973) 6216.
[11] W. Roy Mason, A Practical Guide to Magnetic Circular Dichroism Spectroscopy, Willey–Interscience, Hoboken, 2007.
[12] (a) B. Holmquist, T.A. Kaden, B.L. Vallee, Biochem 14 (1975) 1454; (b) T.A. Kaden, B. Holmquist, B.L. Vallee, Inorg. Chem. 13 (1974) 2585; (c) T.A. Kaden, B. Holmquist, B.L. Vallee, Biochem. Biophys. Res. Commun. 46 (1972) 1654.
[13] (a) H. Kato, K. Akimoto, J. Am. Chem. Soc. 96 (1974) 1351; (b) R.G. Denning, J.A. Spencer, Symp. Farad. Soc. 3 (1969) 84; (c) B.D. Bird, B. Briat, P. Day, J.C. Rivoal, Symp. Farad. Soc. 3 (1969) 70; (d) R.G. Denning, J. Chem. Phys. 45 (1966) 1307.
[14] J.E. Coleman, R.V. Coleman, J. Biol. Chem. 247 (1972) 4718.
[15] M.T. Werth, S.-F. Tang, G. Formicka, M. Zeppezauer, M.K. Johnson, Inorg. Chem. 34 (1995) 218.
[16] M.L. Brader, N.C. Kaarsholm, S.E. Harnung, M.F. Dunn, J. Biol. Chem. 272 (1997) 1088.
[17] S. Suzuki, S. Hirose, S. Sawade, N. Nakahara, Inorg. Chim. Acta 108 (1985) 155.
[18] M. Hüber, L. Bubacco, M. Beltramini, B. Salvato, H. Elias, J. Peisach, E. Larsen, S.E. Harnung, W. Haase, Inorg. Chem. 35 (1996) 7482.
[19] F.B. Johansson, A.D. Bond, U.G. Nielsen, B. Moubaraki, K.S. Murray, K.J. Berry, J.A. Larrabee, C.J. McKenzie, Inorg. Chem. 47 (2008) 5079.
[20] (a) J. Krzystek, S.A. Zvyagin, A. Ozarowski, A.T. Fiedler, T.C. Brunold, J. Telser, J. Am. Chem. Soc. 126 (2004) 2148; (b) J. Lawrence, C.C. Beedle, E.-C. Yang, J. Ma, S. Hill, D. Hendrickson, Polyhedron 26 (2007) 2299.
[21] B.P. Yang, A.V. Prosvirin, Y.-Q. Guo, J.-G. Mao, Inorg. Chem. 47 (2008) 1453.
[22] D.M. Duggan, D.N. Hendrickson, Inorg. Chem. 14 (1975) 1944.
[23] J.M. Herrera, A. Bleuzen, Y. Dromzée, M. Julve, F. Lloret, M. Verdaguer, Inorg. Chem. 42 (2003) 7052.
[24] (a) U. Beckmann, S. Brooker, C.V. Depree, J.D. Erwing, B. Moubaraki, K.S. Murray, Dalton Trans. (2003) 1308; (b) S. Brooker, D.J. de Geest, R.J. Kelly, P.G. Plieger, B. Moubaraki, K.S. Murray, G.B. Jameson, Dalton Trans. (2002) 2080.
[25] A. Caneschi, A. Dei, D. Gatteschi, V. Tangoulis, Inorg. Chem. 41 (2002) 3508.
[26] G. De Munno, M. Julve, F. Lloret, J. Faus, A. Caneshi, J. Chem. Soc., Dalton Trans. (1994) 1175.
[27] O. Fabelo, J. Pasan, F. Lloret, M. Julve, C. Ruiz-Perez, Inorg. Chem. 47 (2008) 3568.
[28] G. Aromi, H. Stoeckli-Evans, S.J. Teat, J. Cano, J. Ribas, J. Mater. Chem. 16 (2006) 2635.
[29] D. Kong, Y. Li, X. Ouyang, A.V. Prosvirin, H. Zhao, J.H. Ross Jr., K.R. Dunbar, A. Clearfield, Chem. Mater. 16 (2004) 3020.
[30] (a) Q. Zhao, H. Li, Z. Chen, R. Fang, Inorg. Chim. Acta 336 (2002) 142; (b) F.J. Rietmeijer, G.A. van Albada, A.J. den Hartog, J. Reedijk, Inorg. Chem. 24 (1985) 3597; (c) L.R. Groeneveld, R.A. le Febre, R.A.G. de Graaff, J.G. Haasnoot, G. Vos, J. Reedijk, Inorg. Chim. Acta 102 (1985) 69; (d) F.J. Rietmeijer, J.G. Haasnoot, A.J. den Hartog, J. Reedijk, Inorg. Chem. 113 (1986) 147.
[31] A.C. Rizzi, C.D. Brondino, R. Calvo, R. Baggio, M.T. Garland, R.E. Rapp, Inorg. Chem. 42 (2003) 4409.
[32] H. Kumagai, Y. Oka, S. Kawata, M. Ohba, K. Inoue, M. Kurmoo, H. Okawa, Polyhedron 22 (2003) 1917.
[33] (a) M. Murrie, S.J. Teat, H. Stæckli-Evans, H.U. Güdel, Angew. Chem. Int. Ed. 42 (2003) 4653; (b) K.W. Galloway, A.M. Whyte, W. Wernsdorfer, J. Sanches-Benitez, K.V. Kamenev, A. Parkin, R.D. Peacock, M. Murrie, Inorg. Chem. 47 (2008) 7438.
[34] P.D.W. Boyd, M. Gerloch, J.H. Harding, R.G. Woolley, Proc. R. Soc. Lond. A 360 (1978) 161.
[35] S.M. Ostrovsky, K. Falk, J. Pelikan, D.A. Brown, Z. Tomkowicz, W. Haase, Inorg. Chem. 45 (2006) 688.
[36] K. Fink, C. Wang, V. Staemmler, Inorg. Chem. 38 (1999) 3847.
[37] A.V. Palii, B.S. Tsukerblat, E. Coronado, J.M. Clemente-Juan, J.J. Borras-Almenar, J. Chem. Phys. 118 (2003) 5566.
[38] M.E. Lines, J. Chem. Phys. 55 (1971) 2977.
[39] Z. Tomkowicz, S. Ostrovsky, H. Mueller-Bunz, A.J. Hussein Eltmimi, M. Rams, D.A. Brown, W. Haase, Inorg. Chem. 47 (2008) 6956.
[40] F. Lloret, M. Julve, J. Cano, R. Ruiz-Garcia, E. Pardo, Inorg. Chim. Acta 361 (2008) 3432.
[41] V.S. Oganesyan, S.J. George, M.R. Cheesman, A.J. Thomson, J. Chem. Phys. 110 (1999) 762.
[42] F. Neese, E.I. Solomon, Inorg. Chem. 38 (1999) 1847.
[43] E.J.L. McInnes, E. Pidcock, V.S. Oganesyan, M.R. Cheesman, A.K. Powell, A.J. Thomson, J. Am. Chem. Soc. 124 (2002) 9219.
[44] A.V. Palii, S.M. Ostrovsky, S.I. Klokishner, O.S. Reu, Z.-M. Sun, A.V. Prosvirin, H.-H. Zhao, J.-G. Mao, K.R. Dunbar, J. Phys. Chem. A 110 (2006) 14003.
[45] W. Haase, M. Zeppezauer, S. Ostrovsky, Z. Tomkowicz, in press.

[46] W.A. Spoffordtert, P. Boldrini, E.L. Amma, P. Carfagno, P.S. Gentile, J. Chem. Soc. D (1970) 40.
[47] R. Herchel, personal communication.
[48] D.A. Brown, W. Errington, W.K. Glass, W. Haase, T.J. Kemp, H. Nimir, S.M. Ostrovsky, R. Werner, Inorg. Chem. 40 (2001) 5962.
[49] U. Turpeinen, R. Hämäläinin, J. Reedijk, Polyhedron 6 (1987) 1603.
[50] S.M. Ostrovsky, R. Werner, D.A. Brown, W. Haase, Chem. Phys. Lett. 353 (2002) 290.
[51] W. Haase, in press.
[52] V. Calvo-Perez, personal communication.
[53] V. Calvo-Perez, S. Ostrovsky, A. Vega, J. Pelikan, E. Spodine, W. Haase, Inorg. Chem. 45 (2006) 644.